

Utilization of Carbon-Embedded Photocatalysts Prepared at Different Oxidation Conditions for Gaseous Methyl Tertiary-butyl ether Decomposition†

JUN-YEOP LEE and WAN-KUEN JO*

Department of Environmental Engineering, Kyungpook National University, 80 University Road, Bukgu, Daegu 702-701, Republic of Korea

*Corresponding author: Fax: +82 53 9506579; Tel: +82 53 9506584; E-mail: wkjo@knu.ac.kr

AJC-13347

The present study investigated the surface and morphological characteristics and the photocatalytic activities of carbon-embedded photocatalysts for the purification of in-vehicle level methyl tertiary-butyl ether under different experimental conditions. This decomposition was achieved using titanium carbide (TiC) and five photocatalysts prepared by oxidizing TiC at different oxidation temperatures (250, 300, 350, 400 and 450 °C, which were designated as TiC-250, TiC-300, TiC-350, TiC-400 and TiC-450, respectively). Their characteristics were determined using a variety of spectral instruments. The surface area, pore volume and carbon content of pure TiC and as-prepared photocatalysts were also determined. For the pure TiC and TiC-250, the photocatalytic decomposition for methyl tertiary-butyl ether was close to zero, whereas the other photocatalysts revealed certain degrees of photocatalytic decomposition efficiency. XRD pattern exhibited that TiO₂ crystal phases were not formed for the TiC and TiC-250, indicating that these two types of powders could not have any photocatalytic functions for methyl tertiary-butyl ether decomposition. TiC-300 showed the highest methyl tertiary-butyl ether decomposition efficiency (average value of 82 %), followed by TiC-350 (average value of 77 %), TiC-400 (average value of 44 %) and TiC-450 (average value of 8 %). Consequently, the as-prepared photocatalysts could effectively be applied for airborne methyl tertiary-butyl ether purification inside vehicles, when their preparation conditions were optimized.

Key Words: Oxidation temperature, Photocatalytic decomposition, Operational condition, In-vehicle level.

INTRODUCTION

A number of researchers have prepared C-TiO₂ photocatalysts using a variety of synthesis processes, such as chemical vapour deposition¹, thermal oxidation of titanium carbide², sol-gel processes³ and hydrothermal⁴. They reported that as-prepared C-TiO₂ photocatalysts revealed high photocatalytic performance under visible-light irradiation conditions. The C-TiO₂ photocatalysts extend effectively the light absorbance into the visible region primarily due to its unique electrical as well as structural properties. The carbon dopant has been described to be a substitutional anion, which is associated with the -4 oxidation state in the Ti-C bond in carbide, or as an interstitial cation, which is associated with the +4 oxidation state in the C-O bond in carbonates⁵. These oxidation states are ascribed to the band gap narrowing of TiO₂ or the formation of localized mod-gap state, thereby extending the light absorbance of C-TiO₂ into visible-light region⁶. In addition, C-TiO₂ is likely to reduce the electron-hole recombination which in practice can reduce the effectiveness of TiO₂ as a heterogeneous photocatalyst⁷.

Previous photocatalytic performance tests were carried out primarily in the aqueous phase for the decomposition of water pollutants such as 4-chlorophenol, Reactive Brilliant Red X-3B, methyl orange, methylene blue, phenol, rhodamine B and trichloroacetic acid. However, both the light absorbance of photocatalysts and the reaction kinetics of environmental pollutants are not same at the liquid-solid and gas-solid interfaces. For gas-solid photocatalytic reactions, the photocatalytic performance depends mainly on concentrations and types of gas-phase compounds, air flow rate, light intensity and humidity. On the other hand, major parameters for liquid-solid photocatalytic reactions involve ions, pH, concentrations and types of water pollutants and light intensity^{8,9}. These differences imply that the photocatalytic performance obtained from the photocatalysis of aqueous-phase pollutants may not be applicable to those of gas-phase pollutants.

The vehicle cabin has been considered as a potential environment associated with elevated personal exposure to many gas-phase organic compounds¹⁰. Among these pollutants, methyl-tertiary butyl ether has received increasing amounts of attention as regards to the in-vehicle exposure because it

†Presented to the 6th China-Korea International Conference on Multi-functional Materials and Application, 22-24 November 2012, Daejeon, Korea

has been added to unleaded gasoline to increase octane rating and to enhance the combustion efficiency^{11,12}. The addition of methyl tertiary-butyl ether to unleaded gasoline reduces atmospheric CO concentration levels by 10-15 %¹³. However, the methyl tertiary-butyl ether addition resulted in increasing the in-vehicle methyl tertiary-butyl ether levels, thereby elevating the personal exposure of vehicle occupants¹¹. The personal exposure to this compound is of particular concern because it is potentially linked to carcinogenic effects and other adverse health effects, such as dizziness, nausea, irritated eyes and headaches¹⁴. These environmental health effects of methyl tertiary-butyl ether lead to the development of control techniques to decrease health risk of vehicle occupants from in-vehicle air exposure to this pollutant. Consequently, this study assessed the photocatalytic activities of C-TiO₂ photocatalysts for the purification of in-vehicle level methyl tertiary-butyl ether under different experimental conditions to investigate if the as-prepared photocatalysts can be applied for air purification inside vehicles. The photocatalysts were prepared using a thermal oxidation technique under different temperature conditions.

EXPERIMENTAL

Preparation and characterization of photocatalysts:

Titanium carbide powders (TiC) purchased from the Taiji-Ring Co., China were oxidized at five different temperatures (250, 300, 350, 400 and 450 °C) to prepare C-TiO₂ photocatalysts. TiC powders were sprayed uniformly on a glass plate and then oxidized at the specified temperature for 8 h to obtain grey powders. The as-prepared powders, along with the TiC powders, were characterized using X-ray photoelectron spectroscopy pattern, X-ray diffraction, diffuse reflectance UV-VIS-NIR spectra and Fourier transform infrared (FTIR) spectra. X-ray photoelectron spectroscopy patterns were determined using a Thermo VG Scientific Escalab 250 Spectrometer with monochromatized Al K α excitation. XRD patterns were surveyed on a Rigaku D/max-2500 diffractometer with CuK α radiation operated at 40 kV and 100 mA. Visible absorption spectra were identified using a Varian CARY 5G spectrophotometer equipped with an integrating sphere. FTIR analysis was done on a PerkinElmer Spectrum GX spectrophotometer at a resolution of 4 cm⁻¹ in the spectral range of 4000-400 cm⁻¹.

Photocatalytic performance test: The photocatalytic performance of the as-prepared photocatalysts was examined using a cylindrical photocatalytic reactor, which was prepared using a Pyrex tube with a dimension of 4.5 cm inside diameter and 26.5 cm length. The inner surface of the reactor was pasted with the as-prepared photocatalyst or TiC. For this pasting, the powders were ground in a ceramic bowl and mixed with 0.1 M aqueous ethylenediaminetetraacetic acid solution. Deionized water was added to this mixture for dilution. Subsequently, Triton X-100 was added and the mixture was pasted on the Pyrex reactor. The pasted reactor was dried at 100 °C for 0.5 h and then was calcined in an oven for 0.5 h at the same temperature as used for its oxidation.

A daylight lamp was inserted inside the coated reactor, whose geometry allows for a uniform light distribution onto

the surfaces of photocatalysts. The reactor outside was wrapped with aluminum foil to prevent the transmission light loss from the reactor lamp through the Pyrex reactor window and the transmission light gain from room light sources. The standard gas was prepared by injecting methyl tertiary-butyl ether into a mixing apparatus using a syringe pump (KdScientific Model 210) and by mixing with humidified air. This gas flowed above the photocatalyst-coated Pyrex reactor. The humidity level was controlled by making zero-grade air pass through a activated carbon filter, followed by water-contained impingers in a water bath. The relative humidity (RH) was monitored adjacent to the photocatalytic reactor inlet and outlet using a humidity meter. Air flow rate was adjusted using both rotameters and a mass-flow meter.

The photocatalytic activities of the as-prepared photocatalysts were examined under different thermal oxidation temperature conditions. As described above, the photocatalysts were synthesized at five different thermal oxidation temperatures (250, 300, 350, 400 and 450 °C). The operational parameters were fixed to their representative values: thermal oxidation temperature, 350 °C; air flow rate, 0.5 L min⁻¹; input concentration, 0.1 ppm; and RH, 45 %. The visible-light radiation was provided using an 8-W fluorescent daylight lamp (F8T5DL, Youngwha Lamp Co.). The spectrum of this light source was 400-720 nm. The hydraulic diameter (defined as the inside diameter of the cylindrical Pyrex reactor minus the outside diameter of the lamp) of the photocatalytic reactor was 1.0 cm. The coating weight of the C-TiO₂ photocatalyst was approximately 3.3 mg cm⁻². In addition, for comparison the current study investigated the plug-flow reactor coated with pure TiC under the representative experimental conditions.

Air sampling was carried out by filling a clean Tedlar bag at both the reactor inlet and outlet for 10 min with a specified time interval. The collected chemical species were analyzed using a gas chromatograph (Agilent 7890) installed with a flame ionization detector and a fused silica column (Supelco SPB-5). The peak areas for other compounds than methyl tertiary-butyl ether on the chromatogram were negligible; thus, they were neither qualified nor quantified. The quality control program for the measurements of methyl tertiary-butyl ether involved laboratory blank and spiked samples. The method detection limit of methyl tertiary-butyl ether was 0.9 ppb.

RESULTS AND DISCUSSION

Characteristics of as-prepared photocatalysts according to thermal oxidation temperatures: The characteristics of the TiC as well as its oxidized photocatalysts were analyzed utilizing several spectral and analytical instruments. Fig. 1 illustrates the XRD images of the TiC and five photocatalysts prepared by oxidizing TiC at different oxidation temperatures (250, 300, 350, 400 and 450 °C, which were designated as TiC-250, TiC-300, TiC-350, TiC-400 and TiC-450, respectively). Both the pure TiC and the TiC-250 exhibited several TiC-associated peaks, but not any TiO₂-associated peaks. This suggested that TiO₂ crystal phases were not formed during the oxidation of TiC at such a low temperature (250 °C) condition. In contrast, the TiC-300 showed not only one TiC-related peak

at $36.5^\circ 2\theta$, but also an anatase titania phase with a distinct peak at $25.2^\circ 2\theta$ and a rutile titania phase with a distinct peak at $27.4^\circ 2\theta$. For the TiC-350, the peak appeared at $36.0^\circ 2\theta$ is likely due to the overlap of TiC and TiO_2 rutile phase, while the other peaks are attributed to anatase or rutile phases. The photocatalysts prepared at higher temperatures (TiC-400 and TiC-450) revealed an XRD pattern similar to that of the TiC-300, although their peak intensities were not same as the TiC-300. This confirms that TiO_2 crystal phases were formed during the oxidation of TiC at those high temperature conditions.

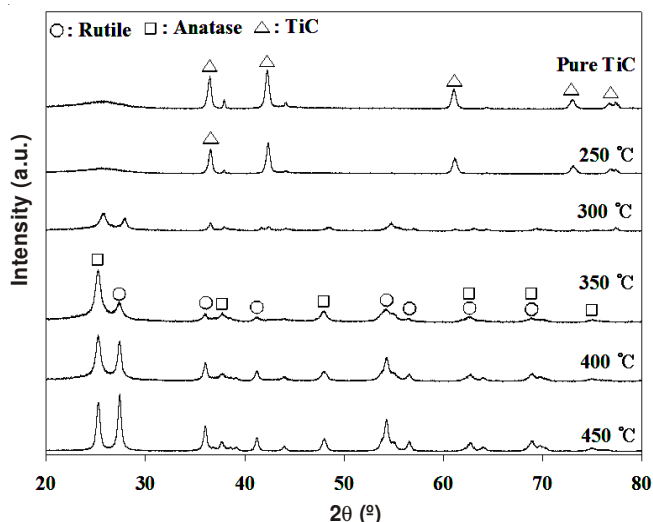


Fig. 1. XRD spectra of TiC and as-prepared photocatalysts by oxidation of TiC at 250, 300, 300, 350 and 450 °C.

Fig. 2 shows the XPS spectra of the TiC and the photocatalysts prepared at different oxidation temperatures. The spectrum of the TiC was deconvoluted to yield five peaks at 290.0, 285.6, 284.5, 284.4 and 281.7 eV. The peak at 281.7 eV is attributed C-Ti contribution¹⁵ and the main peaks at 284.4 and 284.5 eV to the carbon atoms of amorphous carbon matrix¹⁶. The other two peaks at 285.6 and 290.2 eV correspond to the -C-O and -C-O-O bonds, respectively¹⁷. However, the Ti-C peak at 281.7 eV was not observed for the photocatalyst prepared at the oxidation temperatures $\geq 300^\circ\text{C}$, whereas it was appeared for the photocatalyst prepared at 250 °C. This is likely due to the destruction of carbon species at $\geq 300^\circ\text{C}$. This assertion is supported by the TGA results in that the carbon contents decreased gradually with increasing the oxidation temperatures (Table-1).

Table-1 also presents the BET specific surface area and pore volume of the TiC and the oxidized nanocomposites. Based on the N_2 adsorption-desorption isotherm of the nanocomposites, the surface area of the oxidized nanocomposites were less than that of TiC and they decreased with increasing the oxidation temperature. Similar to the XPS result, this is ascribed to the destruction of more carbon species having high surface areas. On the other hand, the specific volume did not depend upon the oxidation temperature, possibly due to the combined effect of the surface area and porosity changes of nanocomposites with oxidation temperature. The volume of TiC-350 exhibited the highest volume ($0.70\text{ cm}^3\text{ g}^{-1}$).

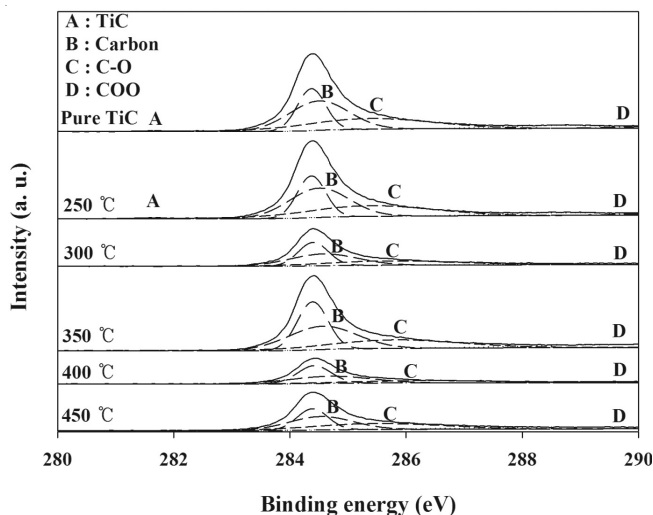


Fig. 2. XPS pattern of TiC and as-prepared photocatalysts by oxidation of TiC at 250, 300, 350, 400 and 450 °C

TABLE-1
BET SURFACE AREA, PORE VOLUME AND CARBON CONTENT OF TiC AND AS-PREPARED PHOTOCATALYSTS BY OXIDATION OF TiC AT 250, 300, 350, 400 AND 450 °C (TiC-250, TiC-300, TiC-350, TiC-400 and TiC-450)

| Type | Area ($\text{m}^2\text{ g}^{-1}$) | Volume ($\text{cm}^3\text{ g}^{-1}$) | Carbon (wt%) |
|---------|-------------------------------------|--|--------------|
| TiC | 333 | 0.48 | 54 |
| TiC-250 | 287 | 0.47 | 54 |
| TiC-300 | 232 | 0.32 | 51 |
| TiC-350 | 213 | 0.70 | 32 |
| TiC-400 | 166 | 0.49 | 26 |
| TiC-450 | 52 | 0.22 | 11 |

Fig. 3 shows the UV-visible absorption spectra of the TiC and the five photocatalysts prepared at different oxidation temperatures. The photocatalyst prepared at the highest oxidation temperature (TiC-450) revealed the absorption edge $\lambda \approx 430\text{ nm}$, which was obtained by extrapolating the linear portion of the absorption edge to the abscissa, similar to that of Degussa P25 TiO_2 , which was reported by previous studies^{18,19}. This indicates that carbonaceous species could not be embedded effectively into TiO_2 at such a high oxidation temperature, likely due to the destruction of carbon contents. In contrast, the absorption edge of photocatalysts prepared at the other lower oxidation temperatures shifted all to the visible-light range. The optical absorption thresholds for the photocatalysts prepared at three low oxidation temperatures (TiC-250, TiC-300 and TiC-350) were $> 700\text{ nm}$ and the threshold of the TiC-400 was approximately 670 nm. These absorption shifts to the visible-light range were ascribed to the presence of carbonate species at interstitial positions of TiO_2 lattice²⁰. This result suggests that the photocatalysts prepared at those oxidation temperatures could be activated under visible-light range. Meanwhile, the absorption edge shifted to more visible-light range with increasing oxidation temperature. This is attributed to more formation of rutile phase at higher oxidation temperature, which has lower band gap energy than anatase phase. This assertion is further supported by the XRD results described above.

The FTIR spectra of the TiC and five photocatalysts prepared at different oxidation temperatures are presented in

Fig. 4. Two bands at 3440 and 1626 cm^{-1} were appeared for the pure TiC as well as all the photocatalysts prepared at between 250 and 450 $^{\circ}\text{C}$. The band at 3440 cm^{-1} corresponds to the O-H stretching vibration, whereas the band at 1626 cm^{-1} results from O-H bending of adsorbed water molecules^{21,22}. Other bands below were also observed for the oxidized photocatalysts, whereas they were negligibly observed for the TiC. These bands were ascribed to the titania crystal lattice vibration^{19,23}. Moreover, the intensities of these two bands increased, as the oxidation temperatures were increased, suggesting more formation of titania crystal phases at high oxidation temperature.

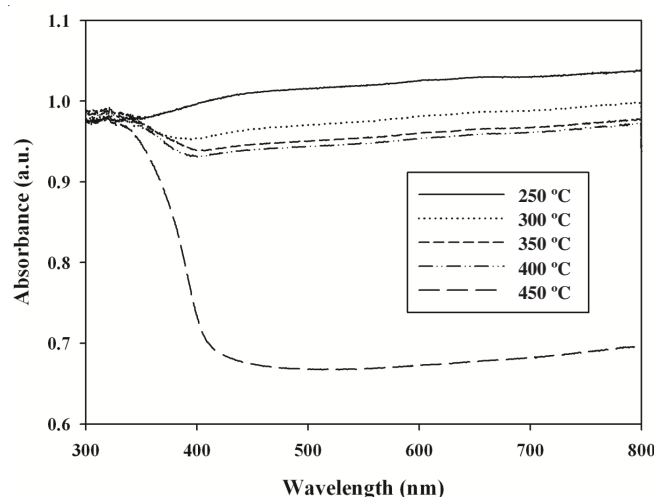


Fig. 3. UV-visible absorption spectra of TiC and as-prepared photocatalysts by oxidation of TiC at 250, 300, 350, 400 and 450 $^{\circ}\text{C}$

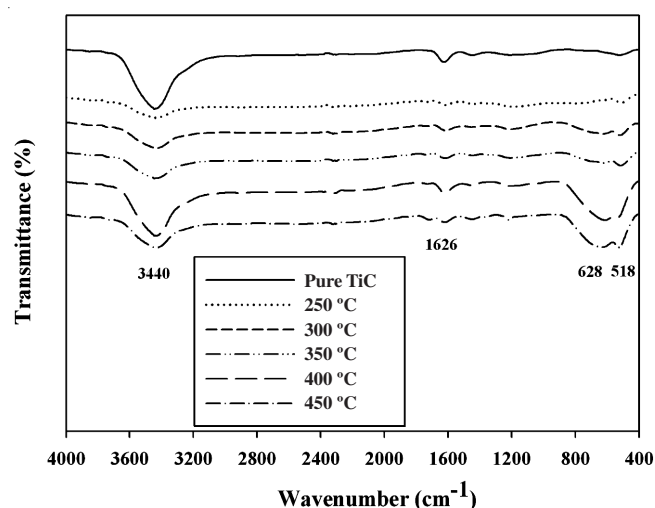


Fig. 4. FTIR spectra of TiC and as-prepared photocatalysts by oxidation of TiC at 250, 300, 350, 400 and 450 $^{\circ}\text{C}$

Photocatalytic activity of prepared photocatalyst under different thermal oxidation temperature conditions: The photocatalytic activities of the as-prepared photocatalysts were determined for gas-phase methyl tertiary-butyl ether control under different thermal oxidation temperature conditions. Five different photocatalysts (TiC-250, TiC-300, TiC-350, TiC-400 and TiC-450) were prepared under different oxidation temperatures. Fig. 5 shows the time-series methyl tertiary-butyl ether decomposition efficiencies determined using pure TiC and the

five prepared photocatalysts. For the pure TiC and TiC-250, the photocatalytic decomposition for methyl tertiary-butyl ether was close to zero, whereas the other photocatalysts revealed certain percentages of photocatalytic decomposition efficiency. As exhibited by the XRD pattern, TiO_2 crystal phases were not formed for the TiC and TiC-250, indicating that these two types of powders could not have any photocatalytic functions for methyl tertiary-butyl ether decomposition. TiC-300 showed the highest methyl tertiary-butyl ether decomposition efficiency (average value of 82 %), followed by TiC-350 (average value of 77 %), TiC-400 (average value of 44 %) and TiC-450 (average value of 8 %). This order is consistent with those for BET surface area and the carbon content of the prepared photocatalysts (Table-1). High BET surface would increase the adsorption sites⁷. For the photocatalysts prepared at higher oxidation temperature, the destruction of the graphite structure of the TiC by the thermal oxidation procedure would reduce the adsorption capacity of the as-prepared photocatalysts, reducing the photocatalytic activity. In addition, high carbon content would increase the amount of carbon dopants thereby extending the light absorbance of C- TiO_2 into visible-light region⁶ and reducing the electron-hole recombination⁷. On the other hand, the pore volumes of TiC-350 and TiC-400 were higher than that for TiC-300, which would result in higher methyl tertiary-butyl ether decomposition efficiency for the two former photocatalysts. Therefore, it was suggested that for the prepared photocatalysts the surface area and carbon content effects on methyl tertiary-butyl ether decomposition efficiency would outweigh the pore volume effect.

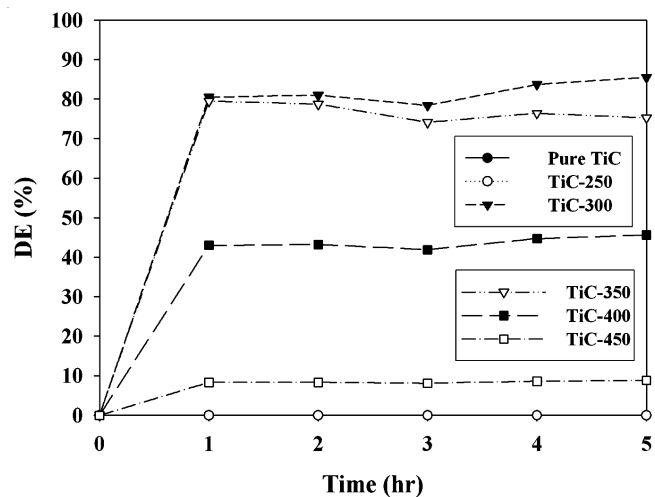


Fig. 5. Time-series methyl tertiary-butyl ether decomposition efficiency (DE, %) determined *via* a photocatalytic system with TiC and as-prepared photocatalysts by oxidation of TiC at 250, 300, 350, 400 and 450 $^{\circ}\text{C}$ (expressed as TiC-250, TiC-300, TiC-350, TiC-400 and TiC-450, respectively)

Conclusion

This study examined the surface and morphological and the photocatalytic activities of carbon-embedded photocatalysts for the purification of in-vehicle level methyl tertiary-butyl ether under different thermal oxidation temperature conditions. The surface and morphological of C- TiO_2 could be successfully determined. The carbon-embedded photocatalysts prepared at

different oxidation conditions exhibited different photocatalytic characteristics and activities for methyl tertiary-butyl ether decomposition. It was suggested that there would be an optimal oxidation temperature for the carbon-embedded photocatalysts synthesized using TiC. Consequently, the as-prepared photocatalysts could be applied effectively to airborne methyl tertiary-butyl ether purification inside vehicles, when their preparation conditions were optimized.

ACKNOWLEDGEMENTS

This work was supported by the National Research Foundation of Korea (NRF) grant funded by the Korean Government (MEST) (No. 2011-0027916).

REFERENCES

1. C.-S. Kuo, Y.-H. Tseng, C.-H. Huang and Y.-Y. Li, *J. Mol. Catal. A*, **270**, 93 (2007).
2. M. Shen, Z. Wu, H. Huang, Y. Du, Z. Zou and P. Yang, *Mater. Lett.*, **60**, 693 (2006).
3. Y. Park, W. Kim, H. Park, T. Tachikawa, T. Majima and W. Choi, *Appl. Catal. B*, **91**, 355 (2009).
4. W. Ren, Z. Ai, F. Jia, L. Zhang, X. Fan and Z. Zou, *Appl. Catal. B*, **69**, 138 (2007).
5. D. Valentin, C. Pacchioni and A. Selloni, *Chem. Matter.*, **17**, 6656 (2005).
6. X. Chen and C. Burda, *J. Am. Chem. Soc.*, **130**, 5018 (2008).
7. R. Leary and A. Westwood, *Carbon*, **49**, 741 (2011).
8. K. Demeestere, J. Dewulf and H. Van Langenhove, *Crit. Rev. Environ. Sci. Technol.*, **37**, 489 (2007).
9. A. Fujishima, X. Zhang and D.A. Tryk, *Surf. Sci. Rep.*, **63**, 515 (2008).
10. O. Geiss, S. Tirendi, J. Barrero-Moreno and D. Kotzias, *Environ. Int.*, **35**, 1188 (2009).
11. J.W. Lee and W.K. Jo, *Sci. Total Environ.*, **291**, 219 (2002).
12. C. Jia, J. D'Souza and S. Batterman, *Environ. Int.*, **34**, 922 (2008).
13. D.M. Mannino and R.A. Etzel, *J. Air Waste Manage. Assoc.*, **46**, 20 (1996).
14. USEPA (United States Environmental Protection Agency), Integrated Risk Information System (IRIS). U.S. Environmental Protection Agency (U.S. EPA) (2005), <http://cfpub.epa.gov/ncea/iris/index.cfm> (accessed 29.11.10).
15. E. Lewin, P.O. Å. Persson, M. Lattermann, M. Stüber, M. Gorgoi, A. Sandell, C. Ziebert, W. Schäfers, W. Braun, J. Halbritter, S. Ulrich, W. Eberhardt, L. Hultman, H. Siegbahn, S. Svensson and U. Jansson, *Surf. Coat. Technol.*, **202**, 3563 (2008).
16. W. Gulbinski, S. Mathur, H. Shen, T. Suszko, A. Gilewicz and B. Warcholinski, *Appl. Surf. Sci.*, **239**, 302 (2005).
17. A.A. El Mel, B. Angleraud, E. Gautron, A. Granier and P.Y. Tessier, *Thin Solid Films*, **519**, 3982 (2011).
18. Z. Wang, W. Cai, X. Hong, X. Zhao, F. Xu and C. Cai, *Appl. Catal. B*, **57**, 223 (2005).
19. W.K. Jo and J.T. Kim, *J. Hazard. Mater.*, **164**, 360 (2009).
20. H. Li, D. Wang, H. Fan, P. Wang, T. Jiang and T. Xie, *J. Colloid Interf. Sci.*, **354**, 175 (2011).
21. F. Dong, H. Wang and Z. Wu, *J. Phys. Chem. C*, **113**, 16717 (2009).
22. X. Lin, F. Rong, X. Ji and D. Fu, *Micropor. Mesopor. Mater.*, **142**, 276 (2011).
23. T. Peng, D. Zhao, K. Dai, W. Shi and K. Hirao, *J. Phys. Chem. B*, **109**, 4947 (2005).